Boundary-Layer Meteorol (2013) 149:19–41
DOI 10.1007/s10546-013-9826-x

ARTICLE

Mean Flow Near Edges and Within Cavities Situated Inside Dense Canopies

Tirtha Banerjee · Gabriel Katul · Stefano Fontan · Davide Poggi · Mukesh Kumar

Received: 23 August 2012 / Accepted: 18 April 2013 / Published online: 19 May 2013

Abstract A streamfunction-vorticity formulation is used to explore the extent to which turbulent and turbulently inviscid solutions to the mean momentum balance explain the mean flow across forest edges and within cavities situated inside dense forested canopies. The turbulent solution is based on the mean momentum balance where first-order closure principles are used to model turbulent stresses. The turbulently inviscid solution retains all the key terms in the mean momentum balance but for the turbulent stress gradients. Both exit and entry versions of the forest edge problem are explored. The turbulent solution is found to describe sufficiently the bulk spatial patterns of the mean flow near the edge including signatures of different length scales reported in canopy transition studies. Next, the 'clearing inside canopy' or the so-called 'cavity' problem is solved for the inviscid and turbulent solutions and then compared against flume experiments. The inviscid solution describes the bulk flow dynamics in much of the zones within the cavity. In particular, the solution can capture the correct position of the bulk recirculation zone within the cavity, although with a weaker magnitude. The inviscid solution cannot capture the large vertical heterogeneity in the mean velocity above the canopy, as expected. These features are better captured via the first-order closure representation of the turbulent solution. Given the ability of this vorticity formulation to capture the mean pressure variations and the mean advective

T. Banerjee (✉) · G. Katul · M. Kumar
Nicholas School of the Environment, Duke University, Durham, NC, USA
e-mail: tirtha.b@duke.edu

M. Kumar
e-mail: mukesh.kumar@duke.edu

G. Katul
Department of Civil and Environmental Engineering, Duke University, Durham, NC, USA
e-mail: gaby@duke.edu

S. Fontan · D. Poggi
Dipartimento di Idraulica, Transporti ed Infrastrutture Civili, Politecnico di Torino, Torino, Italy
e-mail: stefano.fontan@libero.it

D. Poggi
e-mail: davide.poggi@polito.it

acceleration terms, it is ideal for exploring the distributions of scalars and roughness-induced flow adjustments on complex topography.

Keywords Forest edge · Forest gap · Mean recirculation · Mean vorticity · Turbulently inviscid solution

1 Introduction

Flows within and near forest gaps and cavities are becoming increasingly environmental and ecological in scope. Re-colonization of disturbed areas, seed and pollen dispersal, control of pests by vegetated barriers, and risk analysis of gene flow are but sample applications where estimates of the mean flow field, at minimum, is necessary (Nathan et al. 2002, 2011a,b). Any spatial heterogeneity in the stretch of the canopy along the mean wind direction (x), such as the presence of an edge, a clearing, or a gap generates a mean pressure gradient $\mathrm{d}P/\mathrm{d}x$. At some intermediate height above the gap or edge, the mechanical production of turbulent kinetic energy tends to be small as these production terms scale with the inverse of height from the boundary ($1/z$). Hence, the key terms in the mean longitudinal momentum budget at large z generally reduce to the mean pressure gradient and the two advective terms. We call this simplified state a 'turbulently inviscid flow' or simply 'inviscid flow'. However, in the vicinity of the canopy, gradients in turbulent stresses become significant along with $\mathrm{d}P/\mathrm{d}x$. Within the canopy volume but far from any edge, the drag force also becomes a leading term in the mean momentum balance in addition to the turbulent stress gradients and possibly $\mathrm{d}P/\mathrm{d}x$. We refer to the interplay between the pressure gradient, the turbulent stresses, and the drag force as the planar-homogeneous 'turbulent canopy flow'. To what degree the inviscid flow and the turbulent canopy flow, being asymptotic limiting states to the general problem of flow inside forest gaps, dictate the bulk flow properties near gaps and clearing, frames the compass of this work. This question is explored using a combination of a streamfunction-vorticity model and recent flume experiments. The 'turbulent canopy solution' is first tested across a wide range of canopy types in the absence of a non-zero $\mathrm{d}P/\mathrm{d}x$. Next, flow modification near inhomogeneous forest edges is tested by comparing the model runs against published wind-tunnel experiments and large-eddy simulation (LES) studies. After this, the mean flow inside cavities with different boundary configurations is explored using new flume experiments. Both 'inviscid flow' and 'turbulent canopy solution' are implemented for gaps and the zones 'ruled' by the aforesaid flow regimes are analyzed.

The fundamental dynamics of the mean flow near forest edges is often categorized into two types: entry and exit. The entry problem involves modelling the transition of an equilibrated flow above an extensive clearing into an extensive tall uniform forested canopy, while the exit problem considers the flow from such a forest into the clearing. In the entry problem, the upwind flow senses the forest patch by means of a mean pressure field, leading to the generation of a spatially varying $\mathrm{d}P/\mathrm{d}x$. The velocity field responds to the variations in $\mathrm{d}P/\mathrm{d}x$ rapidly by means of advection. The flow decelerates on the windward side of the edge and later adjusts itself due to the canopy drag to some adjustment length scale (Belcher et al. 2003), comparable to the 'impact zone' length scale. Further downstream, the flow homogenizes, with the generation of an internal boundary layer (IBL), which is defined as the flow over a different surface, as it forms within an existing boundary layer (Stull 1990; Garratt 1992). Very far from the forest edge, the flow statistics re-equilibrate with the forest canopy and only vary in the vertical direction. For an exit flow from the forest, as the

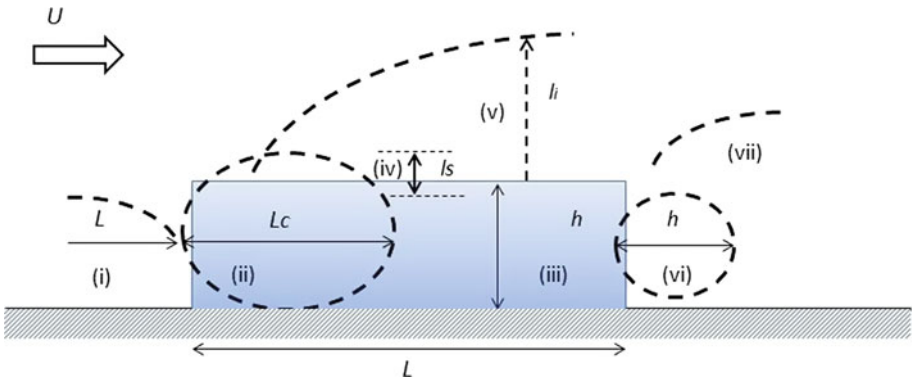

Fig. 1 Schematic showing different zones of adjustment to the canopy transition according to Belcher et al. (2003). (*i*) Impact region; (*ii*) adjustment region; (*iii*) canopy interior; (*iv*) canopy shear layer; (*v*) roughness-change region; (*vi*) exit region; (*vii*) far wake. The quantities h, L, L_c, l_s denote canopy height, length of canopy stretch, adjustment length scale and height of the canopy shear layer respectively

flow departs the forest, it accelerates with occasional recirculation in the case of a denser upstream canopy resembling back-facing step (BFS) flow (Cassiani et al. 2008; Detto et al. 2008). Figure 1 depicts the different zones in the flow with the corresponding internal length scales following Belcher et al. (2003). The impact region, adjustment region, canopy interior, canopy shear layer, roughness change region, exit region and the far wake can be identified in this schematic.

These two configurations are commonly explored using Reynolds-averaged models that employ first-order closure schemes (Li et al. 1990; Peltola 1996), E–ε (Liu et al. 1996) or k–ε (Katul et al. 2004; Frank and Ruck 2008; Dalpe and Masson 2009) to solve for the profiles of the mean velocity and Reynolds stresses inside and above the canopy. These models are routinely compared to wind-tunnel observations and/or field experiments (Raynor 1971; Irvine et al. 1997). Over the last two decades, a number of LES studies have resolved some of the key energetic scales of turbulence inside and around gaps and edges in canopies. These LES studies offer a detailed view of the recirculation regions, re-attachment regions, and their sensitivity to leaf area index (*LAI*) (Yang et al. 2006; Cassiani et al. 2008; Dupont and Brunet 2008; Schlegel et al. 2012). In fact, a classical field study already depicted a recirculation region in a forest clearing by means of smoke drift (Bergen 1975). Recent experimental studies also reported flow adjustment dynamics in the presence of fixed and porous obstructions (Rominger and Nepf 2011). A few LES studies described in detail the development of coherent structures generated due to the canopy transitions (Fesquet et al. 2009; Gavrilov et al. 2010, 2011; Huang et al. 2011) across edges and gaps using fully turbulent theory for the canopy and the space above the canopy as well. Exit flow from a forest or rough-to-smooth transition has been shown experimentally and via LES to be analogous to a BFS problem (Detto et al. 2008; Cassiani et al. 2008). Another study (Belcher et al. 2012) puts forward a comprehensive discussion regarding the influence of complex terrain and forest edges on the mean and turbulent flow statistics, indicating their relevance to the international FLUXNET program for measuring scalar fluxes across regional climates and biomes (Baldocchi et al. 2001). The present work banks on all these results in exploring the problem at hand using a minimalist first-order closure model of turbulence (Holland 1989; Li et al. 1990; Peltola 1996).

2 Theory

2.1 General Considerations

The mean continuity and mean momentum conservation equations for a high Reynolds number, incompressible flow in the absence of Coriolis and buoyancy effects within and above rigid canopies are represented as (Li et al. 1990)

$$\frac{\partial U_i}{\partial x_i} = 0, \tag{1}$$

and

$$\frac{\partial U_i}{\partial t} + \frac{\partial U_i\, U_j}{\partial x_j} = -\frac{1}{\rho}\frac{\partial P}{\partial x_i} + \frac{\partial R_{i\,j}}{\partial x_j} - Fd_i. \tag{2}$$

where U_i are the mean velocity components with $U_1 = U, U_2 = V$, and $U_3 = W$ along directions x_i, where $x_1 = x, x_2 = y$, and $x_3 = z$ are the longitudinal, lateral, and vertical directions, respectively. The coordinate system is aligned so that $U_2 = 0$. The term $U_i\, U_j$ represents the mean advective acceleration terms, ρ denotes the mean fluid density, P denotes the mean departure from hydrostatic pressure and $R_{i\,j}$ denotes the Reynolds stress tensor that encodes the effects of turbulence on the mean flow field, and Fd_i is the drag force in direction x_i induced by the presence of the canopy elements and parametrized as

$$Fd_i = C_\mathrm{d}\, a\, |U|\, U_i = |U|\, U_i / L_\mathrm{c}, \tag{3}$$

where C_d is a dimensionless local foliage drag coefficient that varies between 0.1 and 0.3 for several terrestrial vegetation canopies (Katul et al. 2004), a is leaf area density that can vary appreciably with z depending on the distribution of foliage within the canopy, $|U| = \sqrt{U^2 + W^2}$ is the mean wind speed and L_c is the adjustment length scale.

Upon employing first-order closure principles, the Reynolds stress tensor $R_{i\,j}$ can be written as

$$R_{i\,j} = K_\mathrm{t}\left(\frac{\partial U_i}{\partial x_j} + \frac{\partial U_j}{\partial x_i}\right), \tag{4}$$

where K_t is the turbulent eddy viscosity formulated using a mixing-length model as

$$K_\mathrm{t} = {l_\mathrm{m}}^2 \sqrt{\left(\frac{\partial U_i}{\partial x_j}\right)^2 + \left(\frac{\partial U_j}{\partial x_i}\right)^2}, \tag{5}$$

and where l_m is the canonical mixing length. Following the argument in Wilson and Shaw (1977), l_m is given as

$$l_\mathrm{m} = \min\left(k_\mathrm{v}\, z, \alpha\, h, 2\beta^3 L_\mathrm{c};\ z/h < 1\right) \quad \text{or} \quad k_\mathrm{v}\,(z-d) \tag{6}$$

for $z/h > 1$ where $k_\mathrm{v} = 0.4$ is the von Karman constant, β is a constant related to the attenuation coefficient of the mean velocity varying between 0.1 and 0.3 depending on the canopy density (Campbell and Norman 1998; Poggi et al. 2004), h is canopy height and d is the zero-plane displacement for momentum calculated as the centroid of the drag force (Thom 1971; Jackson 1981; Poggi et al. 2004) in the vertical direction using

$$d = \frac{\int_0^h Fd_1(z)\, z\, \mathrm{d}z}{\int_0^h Fd_1(z)\, \mathrm{d}z}. \tag{7}$$

The premise is that the eddies increase at a rate proportional to $k_v\, z$ from the surface, until they attain a constant size proportional to $\alpha\, h$, where α is a constant that takes the value of $k_v\,(z-d)/h$ to maintain continuity in l_m at the canopy–air interface (but not smoothness). Where the leaf area density $a(z)$ is sufficiently high, eddy sizes are limited by the high concentration of foliage and accounted for by the expression $2\beta^3 L_c$. That is, where $a(z)$ is sufficiently high, the mixing-length is governed by this term, otherwise the constant mixing-length expression $\alpha\, h$ dominates. Thus using the minimum of the three expressions in Eq. 6 can be justified. Taking gradient with respect to x_i to Eq. 2 along with $\partial U_i/\partial x_i = 0$, and rearranging the terms,

$$\frac{1}{\rho}\frac{\partial^2 P}{\partial x_i\, x_i} = -\frac{\partial}{\partial x_i}\left(\frac{\partial U_i\, U_j}{\partial x_j}\right) - \frac{\partial F d_i}{\partial x_i} + \frac{\partial}{\partial x_i}\left(\frac{\partial R_{i\,j}}{\partial x_j}\right). \tag{8}$$

Equation 8 has now the conventional form of a Poisson's equation for P, given as

$$\nabla^2 p = -f \tag{9}$$

where $p = P/\rho$ and f is the negative of the right-hand side of Eq. 8.

2.2 The Mean Streamfunction-Vorticity Representation

Because flows inside cavities, edges, and gaps may be characterized by mean recirculation zones, a vorticity-streamfunction formulation (Pozrikidis 2009) that accommodates the formation of such zones is preferred and can be derived as follows. The U and W mean momentum equations are written separately as

$$\frac{\partial U}{\partial t} + \frac{\partial U\, U}{\partial x} + \frac{\partial U\, W}{\partial z} = -\frac{1}{\rho}\frac{\partial P}{\partial x} + \frac{\partial R_{1\,1}}{\partial x} + \frac{\partial R_{1\,3}}{\partial z} - F d_1, \tag{10}$$

and

$$\frac{\partial W}{\partial t} + \frac{\partial U\, W}{\partial x} + \frac{\partial W\, W}{\partial z} = -\frac{1}{\rho}\frac{\partial P}{\partial z} + \frac{\partial R_{1\,3}}{\partial x} + \frac{\partial R_{3\,3}}{\partial z} - F d_3. \tag{11}$$

where the subscripts 1 and 3 are interchangeably used with the subscripts x and z. Eqs 10 and 11 are differentiated with respect to z and x, respectively and subtracted to obtain the time rate of change of the mean vorticity

$$\frac{\partial \omega}{\partial t} = T_1 + T_2 + T_3 \tag{12}$$

where T_1, T_2, and T_3 include the effects of the advective terms, turbulence, and drag force on the mean vorticity and are given by

$$T_1 = \left(\frac{\partial^2 U\, U}{\partial x\, \partial z} + \frac{\partial^2 U\, W}{\partial z\, \partial z} - \frac{\partial^2 U\, W}{\partial x\, \partial x} - \frac{\partial^2 W\, W}{\partial x\, \partial z}\right), \tag{13}$$

$$T_2 = -\left(\frac{\partial^2 R_{1\,1}}{\partial x\, \partial z} + \frac{\partial^2 R_{1\,3}}{\partial z\, \partial z} - \frac{\partial^2 R_{1\,3}}{\partial x\, \partial x} - \frac{\partial^2 R_{3\,3}}{\partial x\, \partial z}\right), \tag{14}$$

$$T_3 = \left(\frac{\partial F d_1}{\partial z} - \frac{\partial F d_3}{\partial x}\right). \tag{15}$$

The left-hand side of Eq. 12 is the time rate of change of the mean vorticity, defined as

$$\omega = \left(\frac{\partial W}{\partial x} - \frac{\partial U}{\partial z}\right). \tag{16}$$

The mean velocities are related to the mean vorticity through a conventional mean streamfunction. This streamfunction ψ is defined such that

$$U = \frac{\partial \psi}{\partial z}, \tag{17}$$

and

$$W = -\frac{\partial \psi}{\partial x}. \tag{18}$$

The mean streamfunction and the mean vorticity are also linked by a Poisson equation

$$\nabla^2 \psi = -\omega. \tag{19}$$

The algorithm implemented to solve this equation is briefly highlighted in the subsequent section.

2.3 Turbulently Inviscid Scheme

The turbulently inviscid scheme can be described as the condition where the effects of the turbulent Reynolds stress gradients are neglected. The momentum balance equation is thus bereft of the term containing the turbulent diffusivity, which is an analogy to the molecular viscosity in the first-order closure principle and hence the flow is called turbulently inviscid. The term $\frac{\partial R_{ij}}{\partial x_j}$ is dropped from Eq. 2 and therefore its contributions are omitted in the subsequent analysis of the turbulently inviscid scheme. It is to be noted that the gradient of the stress is neglected, not the stress itself and another significant observation is that the governing momentum equation under the inviscid condition is first-order non-linear while its fully turbulent counterpart is second-order non-linear. Hence the turbulent and the inviscid schemes are significantly different from each other.

2.4 Numerical Implementation and Boundary Conditions

A finite difference formulation on an uniform grid is used to solve Eq. 12; the algorithm is outlined in the Appendix. For solving the Poisson equation (Eq. 19), four boundary conditions must be specified. The flow is assumed to be equilibrated with the underlying surface at the entrance and exit locations resulting in the upstream and downstream boundaries to be horizontal and $\partial \psi / \partial x = 0$. At the top boundary, set far from the clearing or cavity, the streamlines are assumed to be parallel to each other and correspond to the outer-layer velocity (U_{out}), assuming U_{out} is planar uniform. Hence, a Dirichlet boundary condition of $\psi = (1/2) \int U_{\text{out}} \, \mathrm{d}z$ is imposed. At the bottom boundary,

$$\frac{\partial \psi}{\partial z} = \frac{u_{*\text{g}}}{kv} \ln\left(\frac{\Delta_z}{z_0}\right) \tag{20}$$

where $u_{*\text{g}}$ is the friction velocity near the ground (or forest floor), Δ_z is the vertical grid spacing ($>z_0$) and z_0 is the roughness length of the surface (not the vegetation). The formulation in Eq. 20 is consistent with the mixing length in Eq. 6.

The pressure Poisson equation, Eq. 9, is solved with the following boundary conditions: $\partial P / \partial x = 0$ at the bottom and $P = 0$ at the other three sides. The vorticity formulation has a number of advantages. First and foremost, it is not implicit. The structure of Eq. 12 allows it to be solved in a conventional, time marching method, as the vorticity only appears on the right-hand side. Moreover, continuity is automatically satisfied in a streamfunction formulation.

The need to update the pressure and the velocity simultaneously is also eliminated in such a scheme. The disadvantages are that such a scheme requires specification of boundary condition on the streamfunction instead of the velocity and hence is not straightforward.

3 Results and Discussions

Prior to addressing the main problem, the model is first evaluated against published uniform canopy experiments and LES presented in the literature. In the first sub-section, results from previous studies on horizontally homogeneous canopies are reported and compared against model runs to assess the model performance when only the Reynolds stresses and the drag force dominate the mean longitudinal momentum balance. This comparison is intended to provide an independent evaluation of the modelled l_{m} across a wide range of leaf area density shapes and canopy heights when the flow is allowed to attain a stationary and planar homogeneous state. Next, flow modifications introduced by dense forest edge(s) are explored via comparisons with previous LES studies, field, and wind-tunnel experiments. In this case, apart from the Reynolds stress and the drag force, the pressure gradient and the advective terms are the key terms in the momentum budget equation (Eq. 2) close to the edge and in the canopy. In the last sub-section, the proposed formulation is employed for the more complex scenario where a combination of porous and solid configurations are used to describe the boundaries of a cavity intended to mimic a forest-gap in a flume. The extent to which the inviscid solution and the full solution agree with laser Doppler anemometry is discussed for porous–porous (P–P), solid–porous (S–P), porous–solid (P–S), and solid–solid (S–S) cavity boundaries.

3.1 Horizontally Homogeneous Canopy

The case of a horizontally homogeneous canopy has been extensively discussed in the context of turbulent closure schemes (or mixing-length specification) (Shaw and Schumann 1992; Katul et al. 2004; Wang 2012). The model runs are presented against field experiments for seven different dense canopies ranging from a short corn canopy to a tall mixed hardwood forest (Fig. 2). The vertical inhomogeneity is large due to the large variability in $a(z)$. The mean horizontal velocity component (U) and the Reynolds stress (R_{13}) profiles are compared against field measurements reported in Katul et al. (2004) and the other original sources such as Amiro (1990) for aspen, spruce and Jack pine, Wilson et al. (1982) for corn, Katul and Albertson (1998) for Loblolly pine, Leuning et al. (2000) for rice, Meyers and Baldocchi (1991) for hardwood and Kelliher et al. (1998) for Scots pine.

The key observations from these comparisons are as follows:

1. The modelled mean velocity within the canopy agrees with field measurements in many cases (see Table 1). The largest disagreements were for the hardwood (HW) canopy cases, where a topography-induced mean pressure gradient (Lee et al. 1994) (not included in the model calculations here) may have been responsible for generating a secondary maximum. Another reason for this mismatch may be attributed to the severe vertical heterogeneity in $a(z)$, which is mostly concentrated in the top one third of the canopy. It should also be noted that several of the disagreements with the field measurements are also evident for the rice (RI) canopy, though these measurements have anomalous noise due to a sequential sampling employed. The comparisons with the stress profiles and the mean velocity profiles are shown in Table 1.

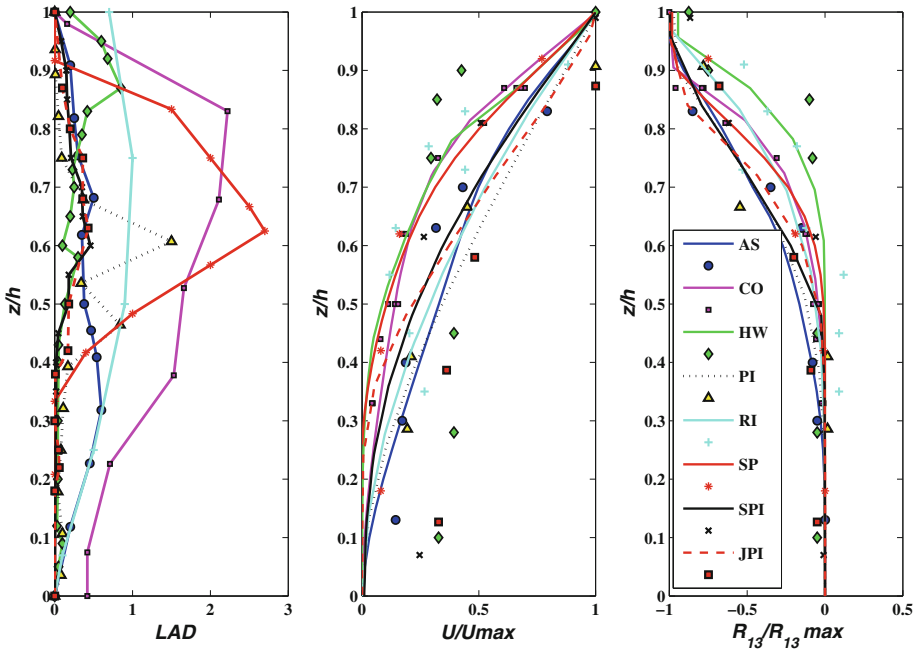

Fig. 2 Leaf area density (*LAD*), normalized mean horizontal velocity $U/U_{\max}$ and normalized Reynolds stress $R_{13}/R_{13\max}$ profiles for seven different vegetation canopies. The canopy types are aspen (*AS*), corn (*CO*), hardwood (*HW*), Loblolly pine (*PI*), rice (*RI*), spruce (*SP*), Scots pine (*SPI*) and Jack pine (*JPI*). The *lines* represent model runs and the markers represent the field measurements cited in Katul et al. (2004). Vertical height z is normalized by the canopy height h. Maximum value is chosen as the normalization reference to provide a uniform basis for comparison among the three parameters. This basis is maintained throughout this study

2. As a whole, it can be stated that the first-order closure model with such a mixing length used to resolve the turbulent features inside the canopy is acceptable for modelling the mean flow. It is to be noted that the present work is not intended to improve the existing canopy turbulence models or their canonical mixing length, but to establish confidence in the model being used in resolving some of the key aspects of turbulence inside canopies.

The results for a horizontally homogeneous canopy have also been compared to a LES study (Shaw and Schumann 1992) and the model runs display similar quality of agreement to these simulations (Fig. 3). It is to be observed that for a homogeneous canopy, vertical profiles of velocity or stress are self-similar at any section. For both *LAI* cases ($LAI = 5$ and 2), the modelled velocity follows LES except in the lower layers of the canopy and close to the ground, while for the stress, the deviations are more significant, particularly above the canopy. However, they follow the same average trend. These results reiterate that the 'turbulent canopy solution' is a plausible approximation.

3.2 Presence of a Forest Edge

Spatial gradients are generated when a forest edge is introduced into an otherwise planar homogeneous flow field. When the flow enters the forest, the pressure increases at the upstream to the entry point and then is reduced as the flow progresses into the forest. The

Table 1 Regression statistics for the one to one comparisons between experimental data (abscissa) and modelled (ordinate) U and R_{13} for horizontally homogeneous canopy

Variable	Species	R^2	Slope	Intercept	*RMSE*
U	AS	0.86	0.81	0.00	0.06
U	CO	0.99	0.93	−0.01	0.01
U	HW	0.01	0.01	0.18	0.02
U	PI	0.94	1.26	−0.01	0.05
U	RI	0.59	0.58	−0.01	0.05
U	SP	0.94	0.87	0.01	0.05
U	SPI	0.76	0.61	0.13	0.04
U	JPI	0.97	0.49	0.17	0.03
R_{13}	AS	0.90	1.04	0.04	0.09
R_{13}	CO	0.98	1.23	−0.01	0.05
R_{13}	HW	0.70	0.86	−0.00	0.14
R_{13}	PI	0.89	0.89	−0.02	0.12
R_{13}	RI	0.72	0.84	0.07	0.13
R_{13}	SP	0.99	0.75	−0.03	0.04
R_{13}	SPI	0.92	0.92	0.06	0.08
R_{13}	JPI	0.99	0.66	−0.08	0.02

The R^2 represents the coefficient of determination and *RMSE* indicates the root-mean-square error in the regression. Slopes and Intercepts for the linear regression are also reported

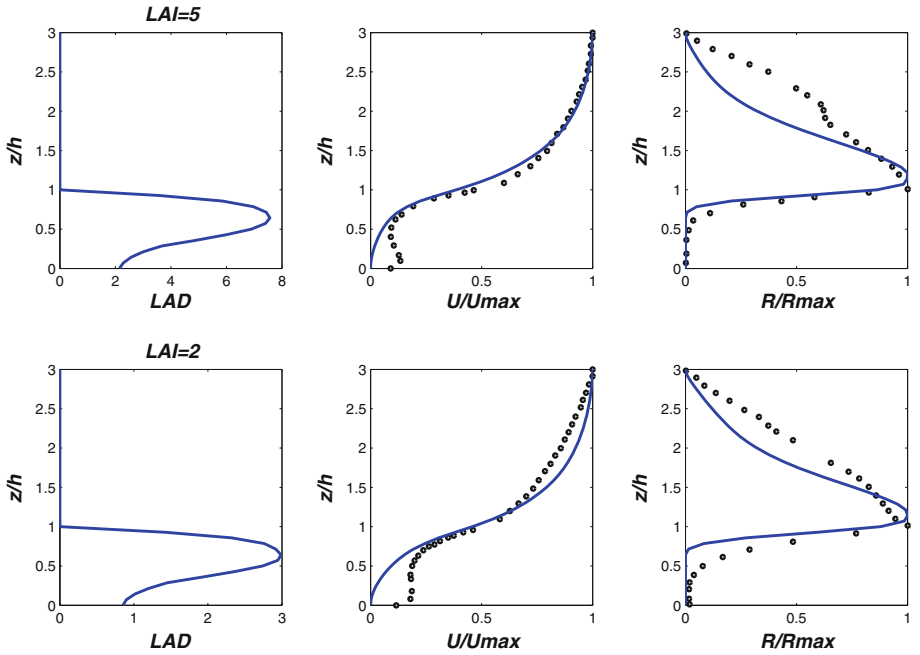

Fig. 3 *LAD*, normalized horizontal mean velocity and normalized Reynolds stress for two different leaf area indices (*LAI*) as indicated in the *figure*. Normalization basis are same as before. *Blue lines* indicate model runs and *black solid dots* indicate LES runs from Shaw and Schumann (1992) digitized by us

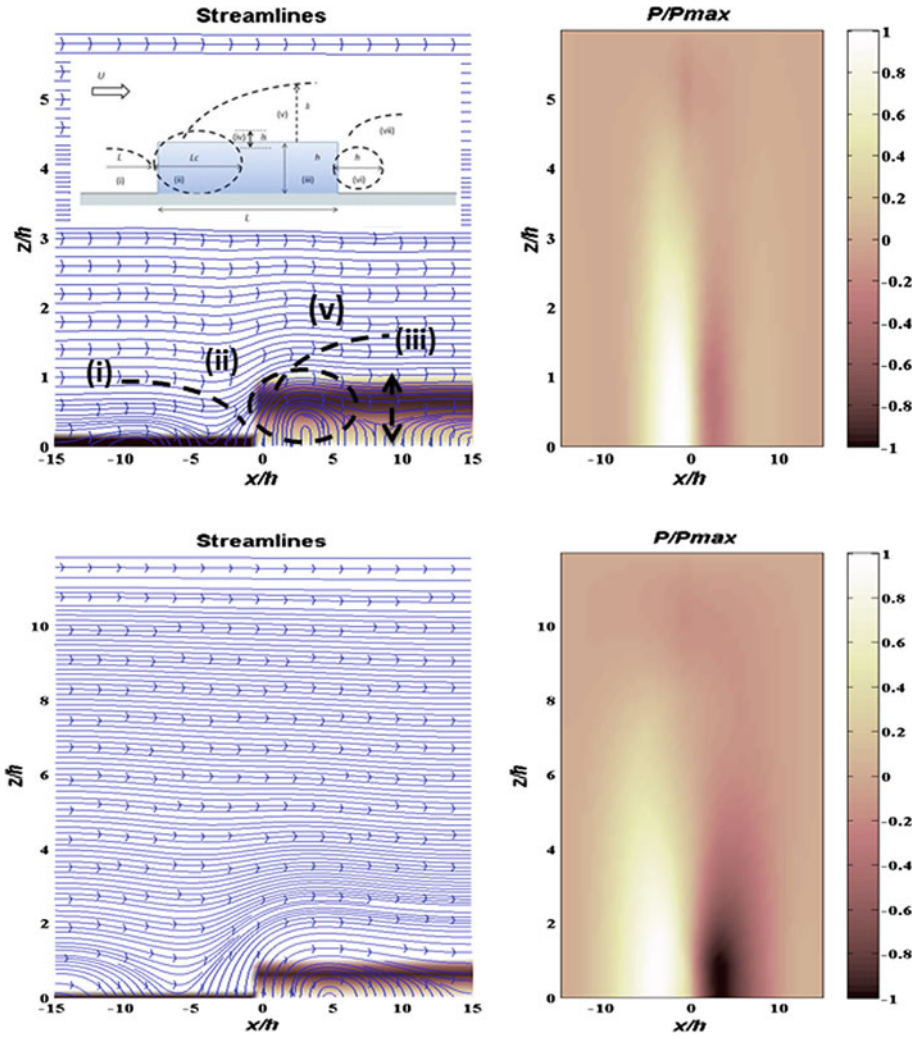

Fig. 4 Computed streamlines and normalized pressure for the forest edge configuration scenario described in Yang et al. (2006). The *colour map* on the streamline plot shows the position of the canopy in terms of the leaf area density. The *bottom row* presents the same scenario with a much higher top boundary to show the dependence of the problem to the upper boundary condition which forces the streamlines to be parallel

streamlines become distorted at the edge and a recirculation zone with an observable length scale is generated immediately past the edge. The strength of this recirculation is dependent on the drag of the canopy. Higher C_d amounts to stronger recirculation (Dalpe and Masson 2009). The proposed model formulation is now applied to the edge-problem described in Yang et al. (2006) and the model runs are compared to the wind-tunnel experiments reported by them (Figs. 4, 5). While other experiments have also been reported on the development of turbulence across forest edges, e.g., Morse et al. (2002), it is the comparison between both LES and wind-tunnel data that makes this dataset ideal for our study.

The structure of the domain in a forest entry problem is shown in Fig. 4. The canopy is preceded by a grassland with uniform $a(z)$ that represents a field situation; the canopy $a(z)$

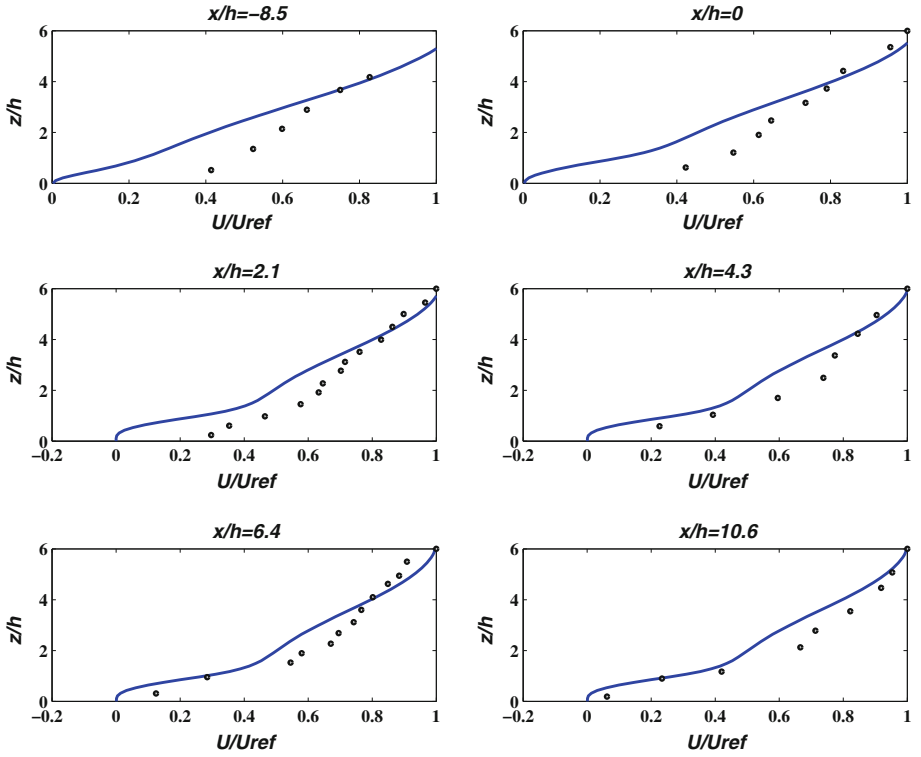

Fig. 5 Normalized velocity profiles at different positions for the forest entry problem described by the wind-tunnel data (Fig. 4) of Yang et al. (2006). The normalization and legend conventions are the same as before

is obtained by digitizing the wind-tunnel data presented in Fig. 4 of Yang et al. (2006). The recirculation zone is clearly visible after the edge and the streamlines become parallel at a height of about $3h$, commensurate with the vertical extent of the canopy sublayer (Raupach and Thom 1981). The distortion of the streamlines upstream of the edge is notable and appears to be a feature in both the model runs presented here and the data presented in Yang et al. (2006). In the bottom row of Fig. 4, the same model runs are presented with the top boundary much higher above the canopy to show the dependence on the upper boundary condition. The upper boundary condition forces zero gradient in the streamlines and the conclusion is that the streamlines become approximately parallel some $3h$ to $5h$ above the ground. However, the mean features of flow distortion around the edge remain the same. The zone of increased pressure and decaying of pressure is shown using a surface plot in Fig. 4. It is to be noted that in the absence of any pressure data, the modelled pressure field is normalized by the maximum pressure to illustrate its relative spatial distribution with respect to the streamlines. The measured and modelled wind profiles (Fig. 5) at the specified sections show acceptable agreement with the LES model runs. The *impact region* upstream of the forest edge, the *adjustment region* immediately downstream of the forest edge and the *roughness change region* downstream and just above the canopy are all visible in Fig. 4. Different zones of flow distortion in a canopy transition according to Belcher et al. (2003) are identified on Fig. 4. The impact region, adjustment region, canopy interior flow and roughness change region can be visually identified in Fig. 4. The length scale L_c, a measure of the efficiency of the canopy to

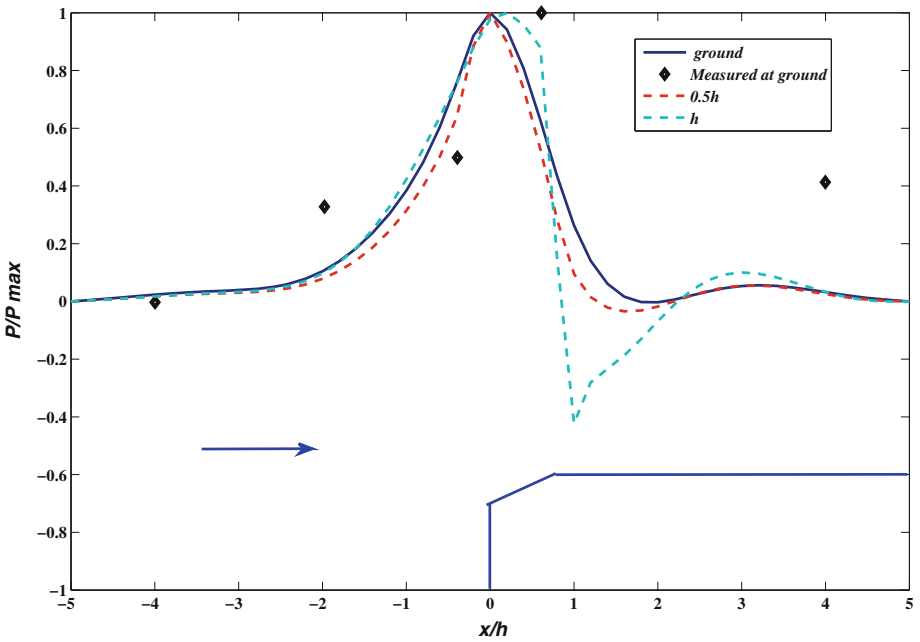

Fig. 6 Normalized surface pressure across a forest edge in an entry problem (*top panel*) described in Nieveen et al. (2001). The *black markers* correspond to field measurements presented in Nieveen et al. (2001) and the *blue lines* depict the computed pressure from the full model. Normalization has been achieved by maximum positive value to provide common basis of comparison. The location and tapered structure of the edge has been qualitatively sketched by the *black lines*. The *solid*, *dashed* and *dotted lines* indicate ground pressure, pressure at half the canopy height and pressure at the canopy height respectively, used to illustrate the magnitude of the vertical pressure variation

remove momentum (Belcher et al. 2003), can be estimated as $L_c/h = (C_d\, LAI)^{-1}$ (Belcher et al. 2003). In particular, the co-location of zones of concentrated vorticity as delineated by the streamlines and the span of the adjustment region determined from L_c ($x/h \approx 2.5$, where $C_d = 0.2$ and $LAI = 2$) is noted in Fig. 4. Moreover, the relaxation of the pressure build-up near the forest edge shown in Fig. 3 occurs over a distance into the forest comparable to $x/h \approx 7.5$, which is also comparable to $x/L_c \approx 3$ noted in Belcher et al. (2003). It is worth mentioning that the pressure field in Fig. 4 is qualitatively similar in terms of the spatial distribution to the entry problem calculations in Li et al. (1990).

A comparison of the modelled pressure has been made with the reported surface pressure measurements in Nieveen et al. (2001) for smooth-to-rough (entry problem) transitions. The forest edge is located at $x/h = 0$. For the entry problem (Fig. 6) negative x/h indicates the grassland before the forest and positive x/h denotes the region inside the forest and past the edge. The edge has a tapered structure as evident from the figure to provide a smoothed and more realistic transition in the entry problem. The field measurements of ground pressure are reported in Nieveen et al. (2001). Pressure at three different levels have been presented in Fig. 6. It is observed that the modelled ground pressure is shifted relative to the measurement by a distance of $0.5h$. The phase relations between longitudinal pressure profiles are also to be noticed. The peak of the pressure pulse has been observed to be at $0.6h$ inside the canopy for the entry problem for both the model run and the measurement. The measurements do not report the decline of pressure immediately past the edge as depicted

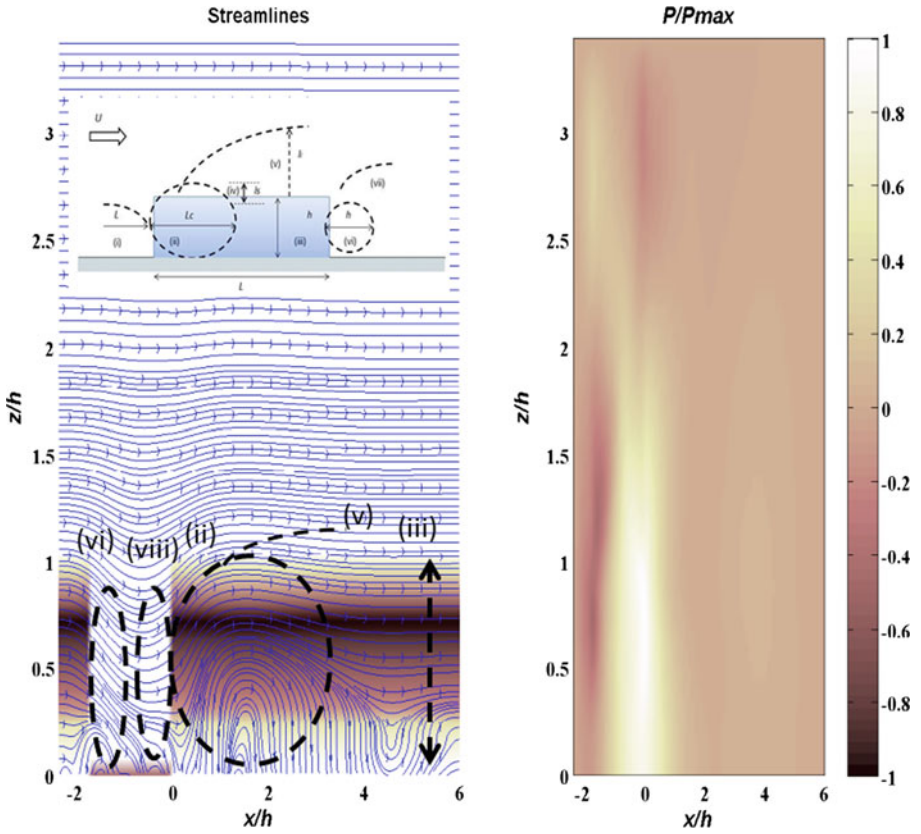

Fig. 7 Computed streamlines and pressure for the problem scenario described in Schlegel et al. (2012). The different zones according to Belcher et al. (2003) are visually identified. An adjustment zone before the second edge is identified as (*viii*)

in the model run. This decrease, however, has been reported by e.g. Wilson and Flesch (1999) and Li et al. (1990). Some of the uncertainties in this comparison can be attributed to lack of knowledge on field conditions (e.g. outer velocity, drag coefficient, leaf area density and distribution near the edge). Also, the model indicates vertical gradients in the horizontal pressure distribution (and their phase relations to the surface across various levels as is evident from Fig. 6).

3.3 Presence of the Gap: Comparison with LES

Moving from a forest entry into a canopy gap configuration, the mean streamfunction-vorticity formulation has been employed to the problem scenario described in Schlegel et al. (2012) and the model runs have been compared to the LES results and field data reported in their study. The $a(z)$ described in that study has been digitized and used in the model. The position of the gap is shown in Fig. 7. The gap in between the canopies is assumed to be a grassland, and the length and height of the domain are normalized by the canopy height. The mean streamlines are now used to describe the flow dynamics in the gap. As the flow exits the forest, a weak recirculation zone appears before the edge. The streamlines illustrate

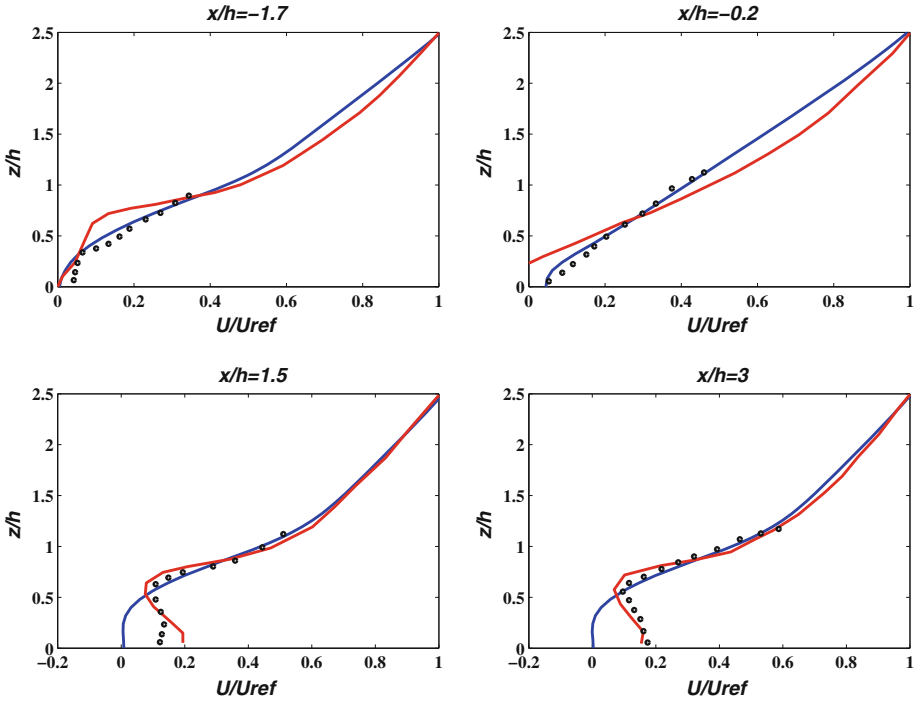

Fig. 8 Normalized velocity profiles at different positions for the problem of flow exiting the forest described in (Fig. 9, HOM case) Schlegel et al. (2012). The *red lines* show the LES data and the *black dots* represent field data. Normalization and legend conventions are the same as before

a concentration of vortices within the lower canopy at the entry. The size of these vortices is commensurate with predictions from Belcher et al. (2003). The streamlines become almost parallel at a height of about $3h$ as before. The different zones of action in a canopy transition are identified in Fig. 7. Adjustment region, canopy interior, roughness change region, exit region and another adjustment region before the gap are identified. The velocity profiles from LES and field data at four qualitatively differently positions are digitized from Schlegel et al. (2012) and they are found to compare well with the computed profiles (Fig. 8), except close to the forest floor. Disagreement between model and data begins at about $0.75h$. Some of these differences are due to lower boundary conditions introduced by the streamfunction formulation and failure of K-theory in this zone.

3.4 Presence of Gap: Comparison with Lab Experiments

Finally, extremes in gap density configuration for the same gap size and bulk flow rate are explored via model calculations suppressing (i.e. inviscid) and activating the turbulent viscosity. The model is run for four different scenarios corresponding to flume measurements, namely P–P, P–S, S–P and S–S configurations, with the flow exiting the first and 'facing' the second. These configurations are intended to amplify or relax pressure perturbations at the two gap interfaces. To retain the same canopy formulation, the solid configuration is modelled using a very high (hundred times the porous case) $a(z)$. This assumption is fair because a very high $a(z)$ implies a near-zero velocity within the mattress (but not pressure).

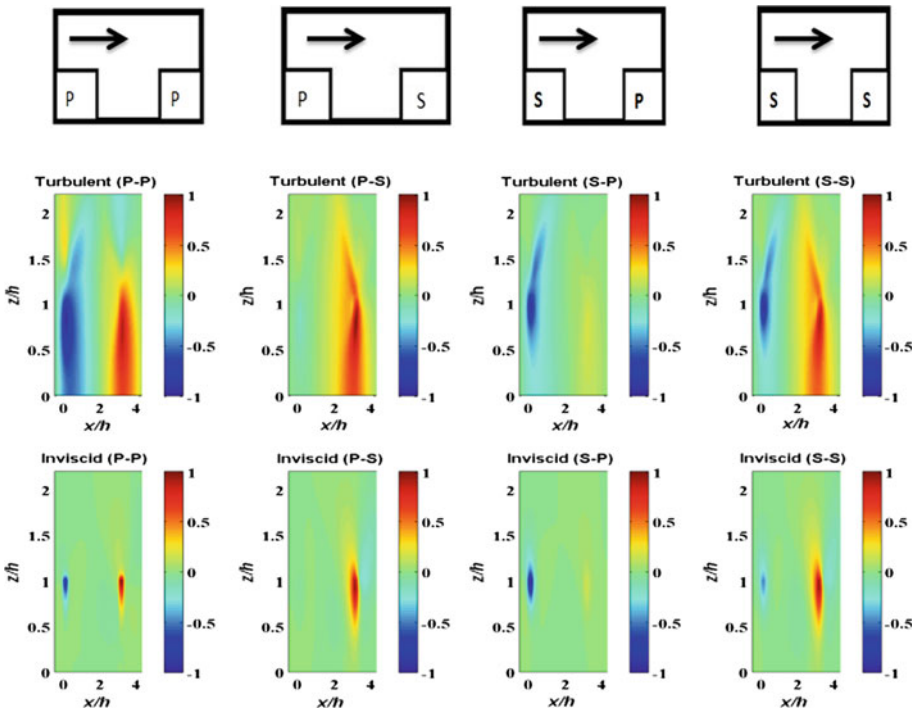

Fig. 9 Normalized pressure fields qualitatively describe the asymmetries originating from different flow configurations for turbulent (*top row*) and turbulently inviscid flow (*bottom row*) and for all four configurations

The experiments have been performed in a large recirculating flume described elsewhere (Fontan et al. 2012). Porous mattresses have been used to simulate the effects of canopy on the flow while the solid mattress was constructed using a stainless steel sheet covering the entire porous mattress. The porous mattresses were composed of open-cell polyurethane foam characterized by a homogeneous and isotropic structure with high permeability. This high permeability allows for the development of a flow resembling a perturbed mixing layer near the porous medium characterizing many dense canopy flows as described in Manes et al. (2011). Laser Doppler anemometry (LDA) was used to acquire the two velocity components at various positions within and above the gap. Dye laser visualization (DLV) runs were used to decide on an optimum gap size. Very small gap size themselves dictate the vortical structure and in a very large gap size, the flow equilibrates after the drop resembling an independent exit, then entry configuration. It has been found that a gap size of $3h$ is 'rich in gap dynamics', that is the configuration 'allows a separated shear layer to be initiated and developed but with a minimum re-attachment zone.' Effectively, the flow is not allowed to equilibrate between re-attachment and the adjustment again. Due to the measurement techniques and materials used, velocity measurements inside the mattress are not possible. To address the primary question here, measured and modelled U, W and R_{13} are compared. For the model runs, the 'full model' and the 'inviscid flow model' outside the mattress domain are also compared. It is recalled that the inviscid model runs are carried out by suppressing the turbulent terms in the two mean momentum budget equations (Eq. 2). Before presenting the mean velocity comparisons, the effects of the gap interfaces on the pressure perturbation are first discussed.

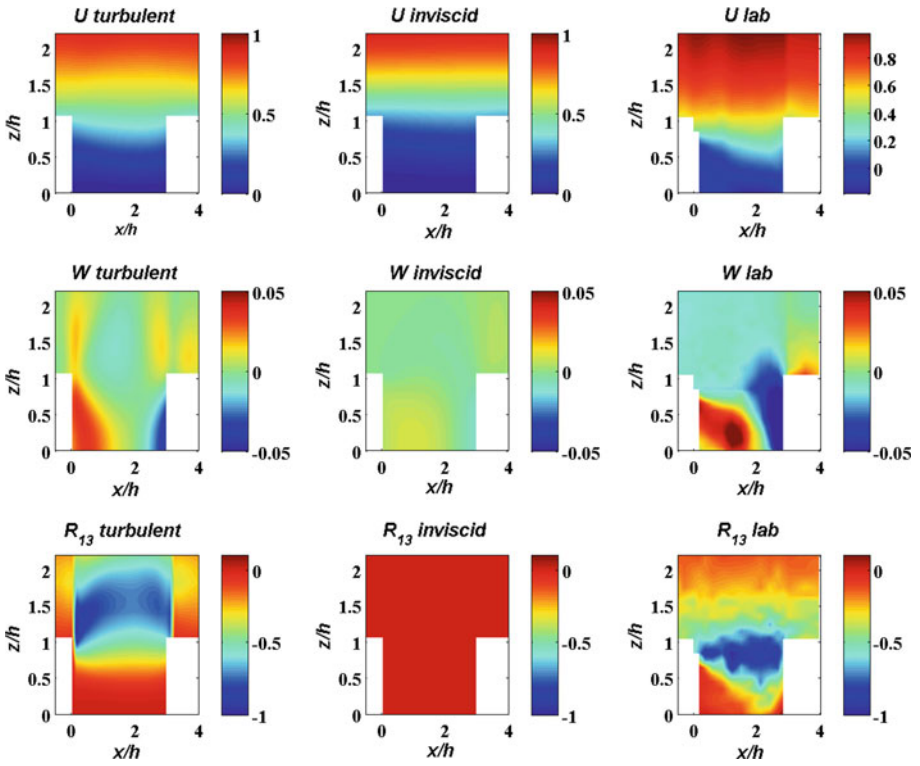

Fig. 10 Spatial variation of mean horizontal and vertical velocity (U and W) components and Reynolds stress (R_{13}) for the P–P configuration. Turbulent and inviscid solutions are presented in the first *two columns*. The *third column* presents the LDA measurements. The U and W are normalized by the maximum U velocity component, i.e., the outer-layer velocity component. This is a logical basis for normalization as the streamlines become parallel at the top of the domain as evident from Fig. 6. R_{13} has been normalized by its maximum value, to provide a common basis of comparison for the experimental and computed data

The computed pressure fields (Fig. 9) for all four configurations demonstrate the sensitivity of the flow to the gap porosity. The pressure features inside the canopy are retained in Fig. 9 for clarity of presentation. The results show:

1. In the case of the P–P configuration, there is a zone of decreased pressure past the exit edge and a zone of increased pressure just before the entrance edge, followed by another zone of decreased pressure. The pressure perturbation intensities are comparable and the pressure field appears quasi-symmetrical about a vertical axis positioned in the centre of the gap.
2. In the case of the P–S configuration, there is a strong zone of increased pressure just before the entrance edge, followed by a zone of decreased pressure. The symmetry noted for the P–P configuration is now broken. The origin of this asymmetry is due to the fact that the solid interface (or the very high leaf area density approximation to it) is far more effective at blocking the flow than the porous interface.
3. In the case of the S–P configuration, there is a zone of strongly decreased pressure past the exit edge and a zone of mildly increasing pressure just before the entrance edge,

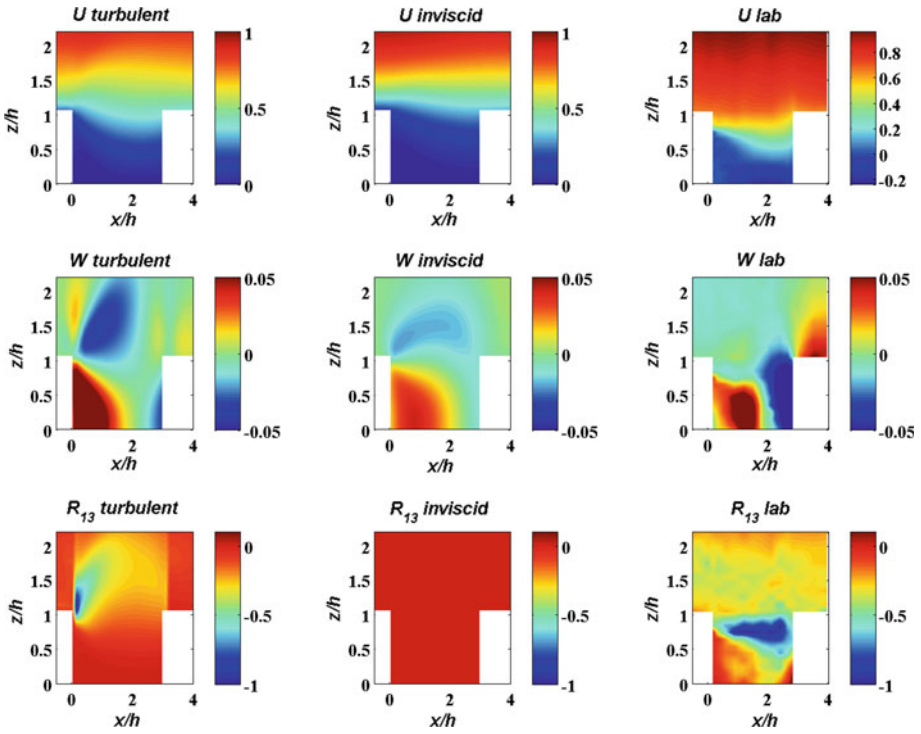

Fig. 11 Spatial variation of mean horizontal and vertical velocity (U and W) components and Reynolds stress (R_{13}) for the S–P configuration. Turbulent and inviscid solutions are presented in the first *two columns*. The *third column* presents the LDA measurements

followed by a zone marked by mild decrease in pressure. The symmetry noted in the P–P configuration is again broken here.

4. In the case of the S–S configuration, there is a zone of decreased pressure past the exit edge and a zone of increased pressure just before the entrance edge, followed by another zone of decreased pressure. The intensities are comparable, but stronger and far more spatially localized than the P–P configuration. Also, the symmetry is restored.
5. The inviscid flow field shows similar trends as the full model that includes the Reynolds stresses, again suggesting that the large-scale pressure perturbations in gaps may be far more influenced by the bulk flow gradients than by the gradients in Reynolds stresses.

How do these pressure perturbations affect the spatial distribution of the two velocity components is discussed next. Only two (P–P and S–P) of the four flow configurations are presented in Figs. 10 and 11 as they illustrate all possible configurational heterogeneity. The results for the P–S and S–S cases were not published previously, though the set-up and Reynolds numbers used are the same as those provided in Fontan et al. (2012). As before, $z/h = 1$ denotes the top of the canopy and the bulk flow is from left to right. The positions of the canopy or solid region appear as white or blocked regions. It is observed that the computed and measured U component reasonably agree. The spatial W fields are moderately comparable but the R_{13} fields are poorly reproduced. The W component increases past the exit-edge and above the entrance-edge, while it decreases above the exit-edge. Inside the gap, the agreement between measured and modelled W component is better than outside.

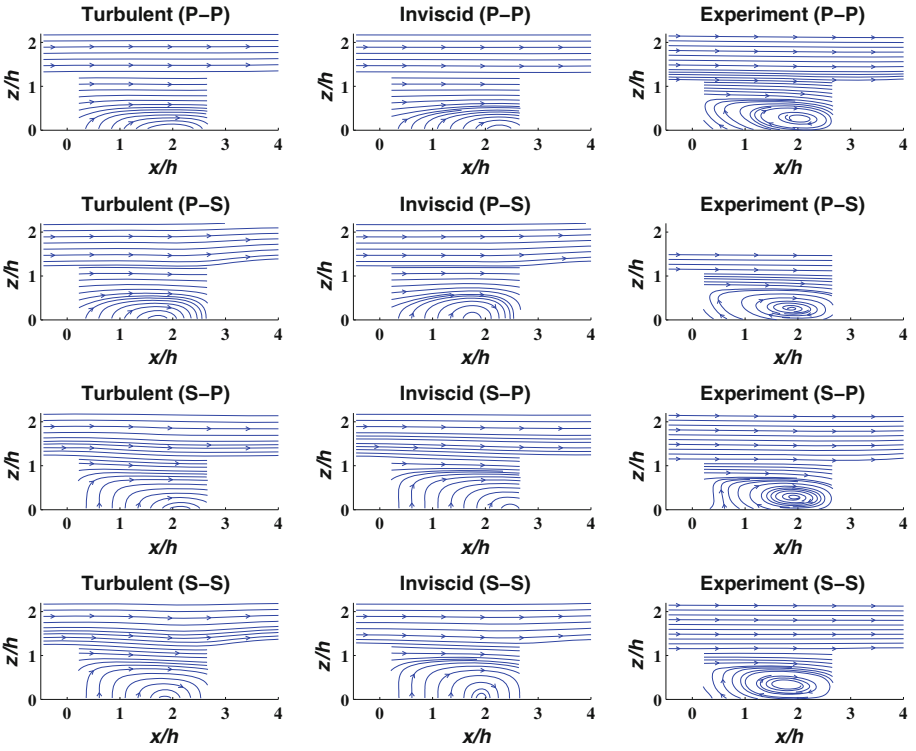

Fig. 12 Streamlines for all four configurations. The *arrows* indicate the direction and magnitude of flow velocity at different positions for different flow configurations. *First column* presents the full solution that includes the turbulent stresses, the *second column* presents the inviscid solution and the *third column* presents the measurements

The mean flow field produced by including the turbulent component is more spatially diffused than the inviscid field (as expected). There is a zone of decreased R_{13} between the two edges. However, this zone is displayed upward for the computed field, compared to the experimental data. This may be caused by a sharply increasing mixing length over and past the canopy, which may be unrealistic for such a configuration. The entire turbulent stress is set to be zero for the inviscid solution across the entire domain because of the zero stress at the water surface. For the P–P configuration, the intensities of the important zones are comparable to each other on the two sides. However, in Fig. 11, the flow transverses past a solid configuration and encounters a porous configuration (the S–P case). Hence the zones marked by an increase and decrease in W are position-wise similar to the P–P case, although characterized by higher intensity. As before, the solution generated by including the turbulent component is more spatially diffused when compared to its inviscid counterpart. It is important to note that, like pressure, W is a good indicator of sensitivity of the flow field to spatial heterogeneity as it is explicitly generated from the spatial variability in the U component.

To emphasize the recirculation regions, streamlines for all the four configurations are presented in Fig. 12. These plots depict a definite recirculation zone in each case with an observable length scale. The flow appears to be more distorted around the solid edges. It is to be noted that the inviscid solution produces the bulk movement of these vectors and offers

Table 2 Regression statistics for the one to one comparisons between experimental data (abscissa) and modelled (ordinate) U and W for two configurations for the complete domain

Variable	Configuration	Solution type	R^2	Slope	Intercept	*RMSE*	t_{slope}	t_{r}
U	P–P	Turbulent	0.96	0.90	0.03	0.07	−185.43	1.69e3
U	P–P	Inviscid	0.93	0.88	−0.01	0.10	−160.93	1.17e3
U	S–P	Turbulent	0.93	0.82	0.01	0.09	−255.98	1.18e3
U	S–P	Inviscid	0.86	0.82	−0.02	0.13	−178.53	0.83e3
W	P–P	Turbulent	0.29	0.21	0.00	0.01	−748.02	210.55
W	P–P	Inviscid	0.52	0.10	0.00	0.00	−2.88e3	345.76
W	S–P	Turbulent	0.20	0.35	0.00	0.02	−299.22	163.33
W	S–P	Inviscid	0.22	0.22	0.00	0.01	−623.58	176.36

The R^2 represents the coefficient of determination and *RMSE* indicates the root-mean-square error in the regression. Slopes and Intercepts for the linear regression are reported. t statistics for slope of unity (t_{slope}) and the correlation coefficient (t_{r}) are also provided

Table 3 Same as Table 1, but only for the cavity domain

Variable	Configuration	Solution type	R^2	Slope	Intercept	*RMSE*
U	P–P	Turbulent	0.84	0.85	0.06	0.14
U	P–P	Inviscid	0.81	0.80	0.03	0.14
U	S–P	Turbulent	0.80	0.76	0.04	0.15
U	S–P	Inviscid	0.75	0.74	0.02	0.17
W	P–P	Turbulent	0.30	0.22	0.00	0.01
W	P–P	Inviscid	0.52	0.10	0.00	0.00
W	S–P	Turbulent	0.21	0.39	0.00	0.02
W	S–P	Inviscid	0.25	0.25	0.00	0.01

a preview of the blue-print or skeleton of the recirculation region within the gap. One to one comparisons for two (P–P and S–P) of the four configurations are provided for both U and W in Tables 2 and 3. Table 2 reports the statistics for the entire problem domain and Table 3 repeats for the gap domain only. It is observed that for all the configurations, the agreement between measured and modelled U component is good, and average to poor for W, though regions of positive and negative W are reasonably delineated by both model calculations. From the *t-statistics*, it is found that the null hypothesis can be rejected in both cases at the 95 % confidence interval, meaning that the correlation coefficient is statistically significant but the model is statistically biased. All these observations reinforce the premise that in the case of a complex flow adjustment problem, the spatial patterns in the bulk flow dynamics may be partly captured by a 'turbulently inviscid' flow. It is well established now that inside the gap, the pressure gradient $\mathrm{d}P/\mathrm{d}x$ governs the flow dynamics. The 'inviscid flow solution' is able to capture the main heterogeneity of the pressure and can propagate it to the mean velocity via the advective terms. This is substantiated by the correct location of the recirculation region in Figs. 10 and 11. The recirculation occurs in a zone below the zone of maximum shear stress at $z/h = 1$. This may be the reason why the inviscid scheme and the turbulent scheme involving K-theory agree in this location.

4 Conclusion

The extent to which turbulent and turbulently inviscid solutions to the mean momentum balance explain the mean flow across forest edges and cavities inside dense forested canopies has been explored. A mean streamfunction-vorticity formulation has been proposed and used to address this question. The advantages of this approach are, (i) guaranteeing conservation of fluid mass, and (ii) capturing recirculation patterns without requiring interactive solutions to the mean velocity and the Poisson equation for pressure. This vorticity formulation has been implemented for a planar homogeneous canopy where the vertical variability in leaf area density has been accounted for. It has been shown that the first-order closure model performance is similar to conventional k–ϵ models inside a canopy lending confidence in the parametrization of the canonical mixing length. Next, the forest edge problem has been explored and the turbulent solution has been found to describe the bulk spatial patterns of the mean flow near the edge. The proposed formulation has been found to predict the signatures of the different length scales observed in a canopy transition as proposed by analytical approaches (Belcher et al. 2003) and as documented by field experiments and LES. Finally, the 'clearing inside canopy' or the so-called 'cavity' problem has been solved for the inviscid and turbulent solutions. It has been found that the inviscid solution can describe the bulk flow dynamics in some intermediate zone inside the cavity. These observations are consistent with the proposition put forward in Belcher et al. (2003, 2012), arguing order of magnitude of the shear stresses is less than that of the so-called inertial or advective terms for much of the flow and even more in the impact region upstream of the edge or in the gap. This implies that the mean flow within the cavity is governed by the horizontal advection rather than the vertical turbulent transport terms. The inviscid solution cannot capture the large vertical heterogeneity in the mean velocity above the canopy, and the more detailed turbulent features within the gap. However, these features can be reasonably captured via first-order closure representations in the turbulent solution. Focusing on the gap region only, both solutions are comparable in terms of agreement with the measurements. Given the ability of this model to capture the pressure variations and the mean advective acceleration terms, it is sufficient for exploring the distributions of scalars and roughness-induced flow adjustments on complex topography.

Acknowledgments Banerjee and Katul acknowledge the support via cooperative agreement (09-ca-11330140-059) from the United States Forest Service (USFS). Katul also acknowledges the support from the National Science Foundation (NSF) (Grants EAR-1013339, AGS-110227, CBET-103347), the US Department of Agriculture (2011-67003-30222), the Binational Agricultural Research and Development (BARD) Fund (Research Grant Award No. IS-4374-11C), the U.S. Department of Energy through the Office of Biological and Environmental Research (BER) Terrestrial Carbon Processes (TCP) program (DE-SC000697) and the Fulbright Italy distinguished scholars program.

Appendix: Numerical Details of the Problems

For solving the systems of equation described in Sect. 2.1, the following algorithm has been used.

1. Initiate U and W fields. For the U field, an exponential profile is used inside the canopy and a logarithmic profile is used above the canopy. W is set to zero uniformly.
2. Initiate the vorticity ω field using the assumed U and W fields using Eq. 16.
3. Find the vorticity at the next timestep using Eq. 12.

Table 4 Numerical details of the problems solved

Problem reference	x/h	z/h	$\mathrm{d}x/h$	$\mathrm{d}z/h$	C_d	*LAI*
Horizontally uniform canopy (Shaw and Schumann 1992)	9.6	3	0.21	0.07	0.15	2–5
Presence of edge (Yang et al. 2006)	30	6	0.67	0.11	0.20	2
Presence of edge (Nieveen et al. 2001)	10	2	0.2	0.04	0.15	2
Presence of gap (Schlegel et al. 2012)	8.4	3.5	0.1	0.08	0.15	7.1
Presence of gap (Fontan et al. 2012)	5	2.8	0.13	0.06	0.30	3.5

4. Using the new vorticity, solve the Poisson equation (Eq. 19) with boundary conditions to obtain the streamfunction ψ at the new timestep.
5. Compute U and W from ψ using Eqs. 17 and 18.
6. Repeat the steps with the new U and W until the differences between successive iterations in vorticity falls below a pre-set tolerance value (usually 5×10^{-3}).
7. Using the converged vorticity, determine the final updated ψ, U and W.
8. Solve the pressure Poisson Eq. 9 to determine $p(x, z)$ using boundary conditions defined afterwards.

The numerical details are listed in Table 4 where $h, x, z, \mathrm{d}x, \mathrm{d}z$ indicate canopy height, horizontal and vertical domain sizes, horizontal and vertical grid spacings, respectively. The grid parameters are normalized by canopy height h. C_d and *LAI* indicate canopy drag coefficient and the canopy *LAI* respectively.

References

Amiro BD (1990) Comparison of turbulence statistics within 3 boreal forest canopies. Boundary-Layer Meteorol 51(1–2):99–121

Baldocchi D, Falge E, Gu LH, Olson R, Hollinger D, Running S, Anthoni P, Bernhofer C, Davis K, Evans R, Fuentes J, Goldstein A, Katul G, Law B, Lee XH, Malhi Y, Meyers T, Munger W, Oechel W, Paw KT, Pilegaard K, Schmid HP, Valentini R, Verma S, Vesala T, Wilson K, Wofsy S (2001) FLUXNET: a new tool to study the temporal and spatial variability of ecosystem-scale carbon dioxide, water vapor, and energy flux densities. Bull Am Meteorol Soc 82(11):2415–2434

Belcher SE, Jerram N, Hunt JCR (2003) Adjustment of a turbulent boundary layer to a canopy of roughness elements. J Fluid Mech 488:369–398

Belcher SE, Harman IN, Finnigan JJ (2012) The wind in the willows: flows in forest canopies in complex terrain. Annu Rev Fluid Mech 44(1):479–504

Bergen JD (1975) Air movement in a forest clearing as indicated by smoke drift. Agric Meteorol 15(2):165–179

Campbell GS, Norman JM (1998) An introduction to environmental biophysics. Springer, New York, 286 pp

Cassiani M, Katul GG, Albertson JD (2008) The effects of canopy leaf area index on airflow across forest edges: large-eddy simulation and analytical results. Boundary-Layer Meteorol 126(3):433–460

Dalpe B, Masson C (2009) Numerical simulation of wind flow near a forest edge. J Wind Eng Ind Aerodyn 97(5–6):228–241

Detto M, Katul GG, Siqueira M, Juang JY, Stoy P (2008) The structure of turbulence near a tall forest edge: the backward-facing step flow analogy revisited. Ecol Appl 18(6):1420–1435

Dupont S, Brunet Y (2008) Edge flow and canopy structure: a large-eddy simulation study. Boundary-Layer Meteorol 126(1):51–71

Fesquet C, Dupont S, Drobinski P, Dubos T, Barthlott C (2009) Impact of terrain heterogeneity on coherent structure properties: numerical approach. Boundary-Layer Meteorol 133(1):71–92

Fontan S, Katul GG, Poggi D, Manes C, Ridolfi L (2012) Flume experiments in turbulent flows across gaps of permeable and impermeable boundaries. Boundary-Layer Meteorol 147:21–39

Frank C, Ruck B (2008) Numerical study of the airflow over forest clearings. Forestry 81(3):259–277

Garratt JR (1992) The atmospheric boundary layer. Cambridge University Press, UK, 316 pp

Gavrilov K, Accary G, Morvan D, Lyubimov D, Bessonov O, Meradji S (2010) Large eddy simulation of coherent structures over forest canopy. Turbul Interact 110:143–149
Gavrilov K, Accary G, Morvan D, Lyubimov D, Meradji S, Bessonov O (2011) Numerical simulation of coherent structures over plant canopy. Flow Turbul Combust 86(1):89–111
Holland JZ (1989) On pressure-driven wind in deep forests. J Appl Meteorol 28(12):1349–1355
Huang J, Cassiani M, Albertson JD (2011) Coherent turbulent structures across a vegetation discontinuity. Boundary-Layer Meteorol 140(1):1–22
Irvine MR, Gardiner BA, Hill MK (1997) The evolution of turbulence across a forest edge. Boundary-Layer Meteorol 84(3):467–496
Jackson PS (1981) On the displacement height in the logarithmic velocity profile. J Fluid Mech 111:15–25
Katul GG, Albertson JD (1998) An investigation of higher order closure models for a forested canopy. Boundary-Layer Meteorol 89(1):47–74
Katul GG, Mahrt L, Poggi D, Sanz C (2004) One- and two-equation models for canopy turbulence. Boundary-Layer Meteorol 113(1):81–109
Kelliher FM, Lloyd J, Arneth A, Byers JN, McSeveny T, Milukova I, Grigoriev S, Panfyorov M, Sogatchev A, Varlargin A, Ziegler W, Bauer G, Schulze ED (1998) Evaporation from a central siberian pine forest. J Hydrol 205(3–4):279–296
Lee XH, Shaw RH, Black TA (1994) Modeling the effect of mean pressure-gradient on the mean flow within forests. Agric For Meteorol 68(3–4):201–212
Leuning R, Denmead OT, Miyata A, Kim J (2000) Source/sink distributions of heat, water vapour, carbon dioxide and methane in a rice canopy estimated using lagrangian dispersion analysis. Agric For Meteorol 104(3):233–249
Li ZJ, Lin JD, Miller DR (1990) Air-flow over and through a forest edge—a steady-state numerical-simulation. Boundary-Layer Meteorol 51(1–2):179–197
Liu J, Chen JM, Black TA, Novak MD (1996) E-epsilon modelling of turbulent air flow downwind of a model forest edge. Boundary-Layer Meteorol 77(1):21–44
Manes C, Poggi D, Ridolfi L (2011) Turbulent boundary layers over permeable walls: scaling and near-wall structure. J Fluid Mech 687:141–170
Meyers TP, Baldocchi DD (1991) The budgets of turbulent kinetic-energy and reynolds stress within and above a deciduous forest. Agric For Meteorol 53(3):207–222
Morse AP, Gardiner BA, Marshall BJ (2002) Mechanisms controlling turbulence development across a forest edge. Boundary-Layer Meteorol 103(2):227–251
Nathan R, Katul GG, Horn HS, Thomas SM, Oren R, Avissar R, Pacala SW, Levin SA (2002) Mechanisms of long-distance dispersal of seeds by wind. Nature 418(6896):409–413
Nathan R, Horvitz N, He YP, Kuparinen A, Schurr FM, Katuk GG (2011a) Spread of North American wind-dispersed trees in future environments. Ecol Lett 14(3):211–219
Nathan R, Katul GG, Bohrer G, Kuparinen A, Soons MB, Thompson SE, Trakhtenbrot A, Horn HS (2011b) Mechanistic models of seed dispersal by wind. Theor Ecol 4(2):113–132
Nieveen JP, El-Kilani RMM, Jacobs AFG (2001) Behaviour of the static pressure around a tussock grassland-forest interface. Agric For Meteorol 106(4):253–259
Peltola H (1996) Model computations on wind flow and turning moment for scots pines along the margins of clear-cut areas. For Ecol Manag 83(3):203–215
Poggi D, Porporato A, Ridolfi L, Albertson J, Katul G (2004) The effect of vegetation density on canopy sub-layer turbulence. Boundary-Layer Meteorol 111(3):565–587
Pozrikidis C (2009) Fluid dynamics: theory, computation, and numerical simulation. Springer, New York, 772 pp
Raupach MR, Thom AS (1981) Turbulence in and above plant canopies. Annu Rev Fluid Mech 13:97–129
Raynor GS (1971) Wind and temperature structure in a coniferous forest and a contiguous field. For Sci 17(3):351–361
Rominger JT, Nepf HM (2011) Flow adjustment and interior flow associated with a rectangular porous obstruction. J Fluid Mech 680:636–659
Schlegel F, Stiller J, Bienert A, Maas HG, Queck R, Bernhofer C (2012) Large-eddy simulation of inhomogeneous canopy flows using high resolution terrestrial laser scanning data. Boundary-Layer Meteorol 142(2):223–243
Shaw RH, Schumann U (1992) Large-eddy simulation of turbulent-flow above and within a forest. Boundary-Layer Meteorol 61(1–2):47–64
Stull RB (1990) An introduction to boundary layer meteorology. Kluwer, Boston, 666 pp
Thom AS (1971) Momentum absorption by vegetation. Q J R Meteorol Soc 97(414):414–428
Wang W (2012) An analytical model for mean wind profiles in sparse canopies. Boundary-Layer Meteorol 142(3):383–399

Wilson JD, Flesch TK (1999) Wind and remnant tree sway in forest cutblocks. III. A windflow model to diagnose spatial variation. Agric For Meteorol 93(4):259–282
Wilson NR, Shaw RH (1977) Higher-order closure model for canopy flow. J Appl Meteorol 16(11):1197–1205
Wilson JD, Ward DP, Thurtell GW, Kidd GE (1982) Statistics of atmospheric turbulence within and above a corn canopy. Boundary-Layer Meteorol 24(4):495–519
Yang B, Raupach MR, Shaw RH, Tha K, Paw U, Morse AP (2006) Large-eddy simulation of turbulent flow across a forest edge. Part I: flow statistics. Boundary-Layer Meteorol 120(3):377–412